Revista Brasileira de Geofísica
RBGf
Brazilian Journal of Geophysics

Revista Brasileira de Geofísica (2015) 33(1): 45-56

ISSN 0102-261X
www.scielo.br/rbg

PLASMA STRUCTURE EXTRACTION FROM LASCO IMAGES BY THE DUAL-TREE COMPLEX WAVELET TRANSFORM

Vitor Moura Souza[1], Margarete Oliveira Domingues[2], Odim Mendes[3] and Aylton Pagamisse[4]

ABSTRACT. Images of the Sun obtained in distinct electromagnetic ranges can be very useful to investigate electrodynamical processes that occur in this star. This work analyzes the application of a two-dimensional version of the Dual-Tree Complex Wavelet Transform (DTCWT) to highlight physical features in the Large Angle and Spectrometric Coronograph images. The importance of those features is that they are related with coronal ejections of magnetized solar plasma, which can produce geomagnetic disturbances at the Earth. The DTCWT is a laborious improvement of the well-known Discrete Wavelet Transform (DWT) with additional properties of shift invariance, ability to analyze multiple directions for multidimensional signals, and computationally efficient algorithms. The multilevel decomposition of an image with the DTCWT generates complex wavelet coefficients, which are manipulated for providing a proper visualization of the plasma structures, highlighting features, and helping further analyses. The methodology implemented here is of interest to space weather laboratories and has been shown to be a very useful tool to a better identification and characterization of the features related to magnetized plasma phenomena in the solar corona.

Keywords: coronal mass ejection, solar plasma, solar corona images, complex wavelet transform, space weather.

RESUMO. Imagens do Sol obtidas em diferentes intervalos do espectro eletromagnético podem ser bem úteis na investigação de processos eletrodinâmicos que ocorrem nesta estrela. Este trabalho analisa a aplicação de uma versão bidimensional da Transformada Wavelet Complexa de dupla árvore (DTCWT) para destacar características físicas nas imagens do Coronógrafo Espectométrico de Ângulo Largo (LASCO). A importância dessas características é que elas estão relacionadas a ejeções coronais de plasma solar magnetizado, que podem produzir perturbações geomagnéticas na Terra. A DTCWT é um aprimoramento laborioso da bem conhecida Transformada Wavelet Discreta (DWT), com propriedades adicionais de: (i) invariância a deslocamentos, (ii) habilidade em analisar múltiplas direções para sinais multidimensionais, e (iii) algoritmo computacionalmente eficiente. A decomposição multinível de uma imagem com a DTCWT gera coeficientes wavelets complexos, que são manipulados para prover uma visualização adequada das estruturas de plasmas, destacando características, e ajudando nas análises posteriores. De interesse dos laboratórios de Clima Espacial, a metodologia implementada aqui mostrou-se ser muito útil para uma melhor identificação e caracterização dos fenômenos de plasmas magnetizados na coroa solar.

Palavras-chave: ejeção de massa coronal, plasma solar, imagens da coroa solar, transformada wavelet complexa, clima espacial.

[1]Instituto Nacional de Pesquisas Espaciais (INPE), Prédio CEA II, Av. dos Astronautas, 1.758, Jd. Granja, 12227-010 São José dos Campos, SP, Brazil. Phone: +55(12) 3208-7865 – E-mail: vitor.souza@inpe.br

[2]Instituto Nacional de Pesquisas Espaciais (INPE), Centro de Tecnologias Especiais (CTE)/Laboratório Associado de Computação e Matemática Aplicada (LAC), Av. dos Astronautas, 1.758, Jd. Granja, 12227-010 São José dos Campos, SP, Brazil. Phone: +55(12) 3208-6542 – E-mail: margarete.domingues@inpe.br

[3]Instituto Nacional de Pesquisas Espaciais (INPE), Ciências Espaciais e Atmosféricas (CEA)/Divisão de Geofísica Espacial (DGE), Av. dos Astronautas, 1.758, Jd. Granja, 12227-010 São José dos Campos, SP, Brazil. Phone: +55(12) 3208-6787 – E-mail: odim.mendes@inpe.br

[4]Universidade Estadual Paulista (UNESP), Faculdade de Ciências e Tecnologia (FCT), Departamento de Matemática, Estatística e Computação (DMEC), Prédio Discente I, Rua Roberto Simonsen, 305, 19060-900 Presidente Prudente, SP, Brazil. Phone: +55(18) 3229-5601 – E-mail: aylton@fct.unesp.br

INTRODUCTION

In several areas identifications or analyses on important features of physical processes can use images. The Large Angle Spectrometric Coronograph (LASCO) aboard the satellite Solar Heliospheric Observatory (SOHO) provides a large number of images of the solar corona, the outer region of the solar atmosphere. By means of that instrument, a device creates an artificial eclipse blocking the solar disk in order to visualize faint corona emissions. Some investigations arising from the analysis of those images concern, for instance, the acceleration of Coronal Mass Ejections (CMEs) (Zhang et al., 2004) and the relationship between the onset times of CMEs and the associated flares (Harrison, 1995; Zhang et al., 2001). As pointed out by (Zhang et al., 2001), the determination of those onset times relies on a high-degree of accuracy in tracking the plasma structures involved. Therefore, it is crucial that structures presented in solar corona images show sharp edges, which are also required for conducting morphological studies (see e.g., St. Cyr et al., 2000, and references therein).

Solar images present hierarchical structures, as discussed in Stenborg et al. (2008) and references therein. By using different physical scales, image analysis may find a myriad of new plasma structures. Hence, image processing techniques based on multiscale properties, such as wavelet transforms, become natural candidates to be applied in those kinds of studies. Stenborg & Cobelli (2003) and Stenborg et al. (2008) have used continuum wavelet transforms with spline wavelet functions and wavelet packets, respectively, in order to improve the visualization of LASCO images.

To the best of our knowledge, no other work has been done for enhancing plasma structures in solar images by means of complex wavelet transforms such as the one we are proposing here. So far, only real wavelet transforms have been used. As a novelty, we use in this work a two-dimensional Complex Wavelet Transform known as Dual-Tree (2D-DTCWT). Thus, the goal is to establish an improved technique in order to unravel or extract hidden plasma structures in originally faint and diffuse features of LASCO images. Here we extend the exploratory analysis presented in our previous work (Moura et al., 2011).

DATASET

The Solar Heliospheric Observatory (SOHO) is a satellite that slowly orbits the L1[5] point, where the combined gravitational forces from Earth and Sun keep SOHO in an orbit locked to the Sun-Earth line (see Fig. 1). Aboard SOHO there are many instruments designed to study the Sun from its deep core to the outer corona and the solar wind. Among them, there is the LASCO instrument which acquires corona images resultant of the white light range of the electromagnetic spectrum. LASCO field of view comprises all plasma phenomena taking place at a distance off the Sun's center ranging from 1.1 to 32 solar radii. The LASCO-C2 telescope covers a distance from 1.5 to 6 solar radii, and the LASCO-C3 telescope covers from 3 to 32 solar radii. Motivated by a comparison with the Stenborg and Cobelli (2003)'s image enhancement method, we chose the following images which are provided by these two telescopes[6]. They are related to the following events:

Event 1. LASCO-C2: eruptive prominence on June 02, 1998 at 13:31 Universal Time (UT);

Event 2. LASCO-C3: coronal mass ejection (CME) on July 04, 2002 at 00:42 Universal Time (UT);

Event 3. LASCO-C2: coronal mass ejection (CME) on August 13, 2002 at 10:54 Universal Time (UT).

All of those images above have a resolution of 1024×1024 pixels and are available in FITS[7] 16-bit format.

These kind of events play an import an role in geomagnetic disturbances at the Earth.

WAVELET TRANSFORMS

Several scientific and technological areas employ wavelet techniques and multiscale analysis, specifically in the development of signal processing and data analysis (Mallat, 1991). According to Selesnick et al. (2005) the success is primarily due to their skills in representing many kinds of real signals which do not often show a good match with the Fourier bases. While the Fourier transform allows only the identification of what frequencies are present in the signal, the wavelet transform provides us with the spatial/temporal localization of those frequencies. In particular, complex wavelet coefficients supply an accurate representation of signals with local abrupt variations (Daubechies, 1992).

Following, we present two kinds of wavelet transforms: the Discrete Wavelet Transform (DWT) and the Dual-Tree Complex Wavelet Transform (DTCWT), and for the latter an extension to a 2-D representation is done. It gives the bases for our processing methodology.

[5]The First Lagrangian Point (L1) is 1.5 million kilometers away from the Earth (about four times the distance from the Moon), in the direction of the Sun.
[6]SOHO archive search at http://seal.nascom.nasa.gov/cgi-bin/gui_seal
[7]FITS: Flexible Image Transport System, more details in http://fits.gsfc.nasa.gov.

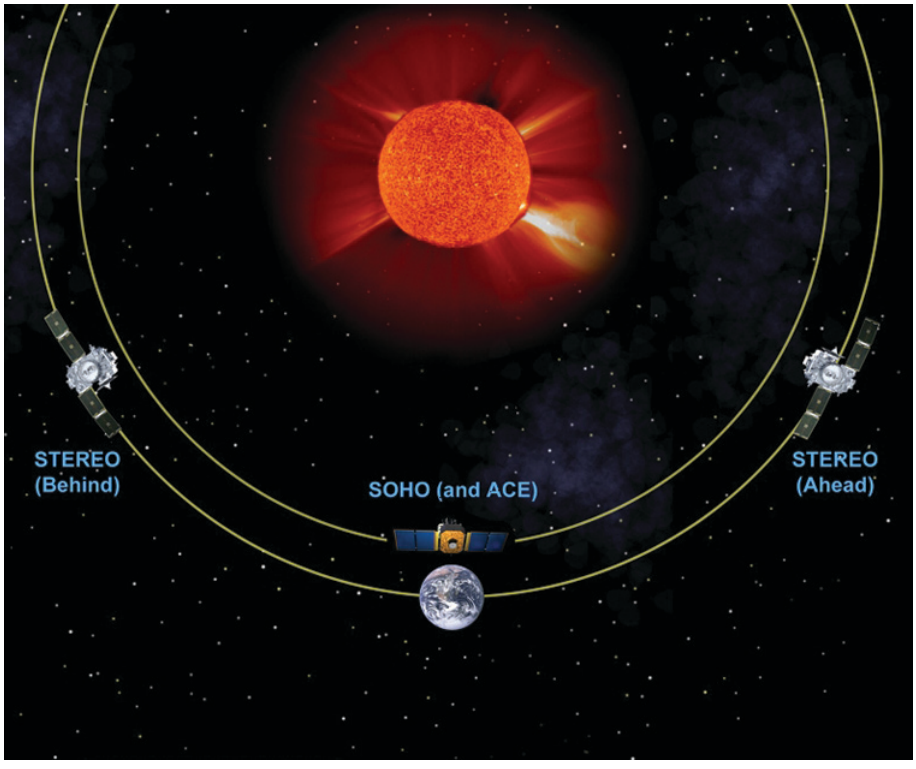

Figure 1 – Illustrative figure (not to scale) showing SOHO orbit. Adapted from: http://stereo.gsfc.nasa.gov.

DWT

Wavelet functions can be build up by the so-called multiresolution analysis introduced by Mallat (1989, 1991). In this framework, the analyzing wavelet function is generated from the scaling function, which obeys the following scale relation, as described in Domingues et al. (2005)

$$\phi(x) = \sqrt{2} \sum_n h(n)\, \phi(2x - n), \tag{1}$$

where $\phi(x)$ is the scale function, and $h(n)$ is a low-pass filter. Then, the analyzing wavelet function becomes

$$\psi(x) = \sqrt{2} \sum_n g(n)\, \phi(2x - n), \tag{2}$$

where $g(n) = (-1)^{n+1} h(1 - n)$ is a high-pass band filter. From this new wavelet $\psi(x)$, it is possible to generate functions $\psi_n^j(x)$ that can be translated and dilated.

The discrete wavelet representation of a real valued signal $f(x) \in \mathcal{L}^2(\mathbb{R})$ is given by:

$$\begin{aligned} f(x) = & \sum_{n=-\infty}^{\infty} c_n\, 2^{j_o/2}\, \phi(2^{j_o} x - n) \\ & + \sum_{j=j_o}^{J_o} \sum_{n=-\infty}^{\infty} d_n^j\, 2^{j/2}\, \psi(2^j x - n), \end{aligned} \tag{3}$$

where $2^{j/2}\, \psi(2^j x - n) \equiv \psi_n^j(x)$ is the bandpass analyzing wavelet, which can be dilated, with the parameter $2^j, j = j_o, j_o + 1, \ldots, J_o$, with J_o (j_o) being the finest (coarsest) scale, and translated, with the parameter $n \in \mathbb{Z}$, generating sets of orthogonal wavelet functions. The same arguments are valid for the low-pass scaling function $2^{j_o/2}\, \phi(2^{j_o} x - n)$. c_n and d_n^j are, respectively, the scale coefficients

$$c_n = 2^{j_o/2} \int_{-\infty}^{\infty} f(x)\ \phi(2^{j_o} x - n)\, dx \tag{4}$$

associated with a smoothing of $f(x)$, and the real valued wavelet coefficients

$$d_n^j = 2^{j/2} \int_{-\infty}^{\infty} f(x)\ \psi(2^j x - n)\, dx, \tag{5}$$

associated with a local regularity of $f(x)$ (Daubechies, 1992).

The fast DWT implementation can be made by using a pyramidal algorithm proposed in Mallat (1989) in which the signal $f(x)$ is convolved with low-pass – $h(n)$ – and high-pass – $g(n)$ – filters, and decimated by a factor of 2, generating the scale and wavelet coefficients, respectively, for each resolution level (Fig. 2).

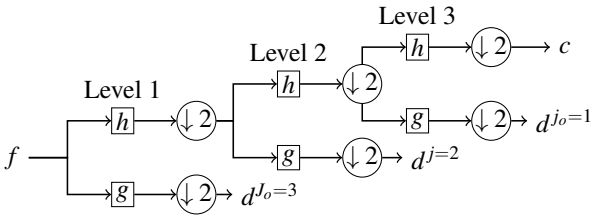

Figure 2 – Mallat's pyramidal algorithm for the forward DWT implementation for three resolution levels. The wavelet coefficients d^j are labeled so that the coarsest scale is $j_o = 1$ and the finest one is $J_o = 3$.

It is possible to retrieve the original signal (perfect reconstruction condition) by performing an inverse DWT (see Fig. 3), in which the input data are both the wavelet and scale coefficients from the coarsest scale obtained in the forward DWT (Fig. 2). The low-pass, $\tilde{h}(n)$, and high-pass, $\tilde{g}(n)$, filters used in the inverse DWT are time-reversed versions of the filters in the forward DWT: $\tilde{h}(n) = h(-n)$, and $\tilde{g}(n) = g(-n)$. In order to retrieve the original signal, an upsampling factor of 2 must be added, at each level, before the convolution of the coefficients with the filters.

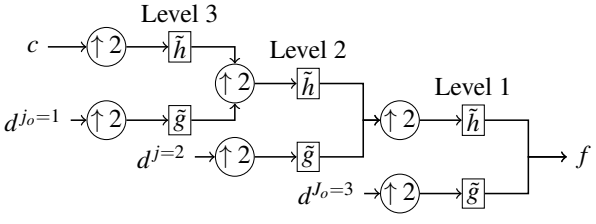

Figure 3 – Mallat's pyramidal algorithm for the inverse DWT implementation for three resolution levels. The wavelet coefficients d^j are labeled so that the coarsest scale is $j_o = 1$ and the finest one is $J_o = 3$.

DTCWT

The DTCWT represents an improvement of the DWT discussed in the previous section, with the following additional properties (Kingsbury, 1998, 2001; Selesnick et al., 2005):

1. **Approximate shift invariance**: shifts in the input signal do not cause major fluctuations in the distribution of energy among the DTCWT coefficients at different scales.

2. **Multiple directionality**: ability for analyzing features for multidimensional signals.

3. **Limited redundancy**: independently on the number of scales.

4. **Efficient order-*N* computation**: only twice the simple DWT for 1-D (2^m times for m-dimensional), and a high computational efficiency as compared to Gabor transform (de Rivaz & Kingsbury, 1999).

The DTCWT generates complex wavelet coefficients by using a dual-tree of wavelet filters to obtain their real and imaginary parts (Kingsbury, 2001). A schematic representation of the forward 1D-DTCWT implementation is shown in Figure 4, in which each tree (a and b) represents one real DWT. In tree a, the real part of complex wavelet coefficients is generated, whereas in tree b the imaginary part is generated. The scale coefficients emerging from each tree are also interpreted as real and imaginary parts of complex scale coefficients. To perform the inverse 1D-DTCWT, the inverse of each of the two DWTs are used to obtain two real signals. These two real signals are then averaged to obtain the reconstructed signal.

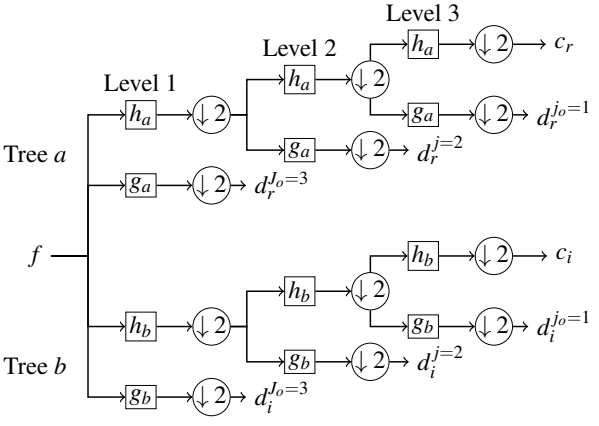

Figure 4 – Schematic view of the 1D-DTCWT implementation for three resolution levels. The subscripts r and i stand for real and imaginary. The wavelet coefficients d^j are labeled so that the coarsest scale is $j_o = 1$ and the finest scale is $J_o = 3$.

The success in accomplishing the DTCWT properties mentioned above relies on the design of the filters of each tree (see Kingsbury, 2001; Selesnick et al., 2005, for more details). At the finest resolution level (Level 1) the low-pass filters of trees a and b in Figure 4 are related by

$$h_b^{(1)}(n) \approx h_a^{(1)}(n-1), \tag{6}$$

where the superscript $^{(1)}$ stands for Level 1, and for the remaining levels (Level 2, and so on)

$$h_b(n) \approx h_a(n-0.5). \tag{7}$$

The filters used in this work are presented in the Appendix. The relation expressed in Eq. (7) is known as the half-sample delay condition. These conditions, relating the low-pass filters from both trees, ensure the approximate analyticity of the complex wavelet

$$\psi_c(x) = \psi_a(x) + i\psi_b(x), \tag{8}$$

where the real valued wavelets $\psi_a(x)$ and $\psi_b(x)$ are related with the high-pass filters from trees a and b, respectively. In

other words, the filters in both trees are jointly designed so that $\psi_b(x)$ is approximately the Hilbert transform of $\psi_a(x)$ (denoted by $\psi_b(x) \approx \mathcal{H}\{\psi_a(x)\}$). The approximate analyticity property guarantees the complex wavelet compact support (or alternatively, its space/time localization) and the approximate fulfillment of the DTCWT properties discussed earlier.

The complex wavelet coefficient $d^j_{c,n}$ is obtained by the projection of the signal $f(x)$ onto $2^{j/2}\psi_c(2^j x - n)$

$$d^j_{c,n} = d^j_{r,n} + i\, d^j_{i,n}, \tag{9}$$

where the subscripts c, r and i stand for complex, real and imaginary. The $d^j_{c,n}$ magnitude is given by

$$\left|d^j_{c,n}\right| = \sqrt{(d^j_{r,n})^2 + (d^j_{i,n})^2} \tag{10}$$

and its phase

$$\angle\, d^j_{c,n} = \tan^{-1}\left[\frac{d^j_{i,n}}{d^j_{r,n}}\right]. \tag{11}$$

These magnitude and phase features can be exploited in multiscale signal processing algorithms (Selesnick et al., 2005). In particular, we shall use an approach which handles with the wavelet coefficient magnitude information giving us a clue for what coefficients must be enhanced in order to highlight the desired plasma structures in LASCO images. We intend to achieve this goal by using an extension of the DTCWT to two dimensions, which is going to be briefly discussed.

DTCWT extension to two-dimension

The DTCWT can be expanded to two or higher dimensions. As the present work is concerned with the analysis of images, we will focus on the two-dimensional version of the DTCWT (2D-DTCWT). This extension can be achieved by separable filtering along columns and then rows. Consider the 2D-wavelet $\psi(x,y) = \psi(x)\,\psi(y)$ associated with this row-column implementation of the wavelet transform, where $\psi(x)$ is a complex approximately analytic wavelet given by Eq. (8). By substituting the complex wavelets $\psi(x)$ and $\psi(y)$ into the expression of $\psi(x,y)$, yields

$$\begin{aligned}\psi(x,y) &= \psi_a(x)\,\psi_a(y) - \psi_b(x)\,\psi_b(y) \\ &+ i\left[\psi_b(x)\,\psi_a(y) + \psi_b(y)\,\psi_a(x)\right].\end{aligned} \tag{12}$$

It is possible to show that both the real part and the imaginary one of Eq. (12) are strongly oriented wavelets (Kingsbury, 2001; Selesnick et al., 2005). In particular, they are oriented at $-45°$. Besides this wavelet shown above, the 2D-DTCWT provides similarly five more complex oriented wavelets. The real parts of these six oriented wavelets can be summarized as follows:

$$\psi_k(x,y) = \psi_{1,k}(x,y) - \psi_{2,k}(x,y), \tag{13a}$$

$$\psi_{k+3}(x,y) = \psi_{1,k}(x,y) + \psi_{2,k}(x,y), \tag{13b}$$

where $k = 1, 2, 3$, $\psi_{1,k}(x,y)$ and $\psi_{2,k}(x,y)$ are given by

$$\begin{aligned}\psi_{1,1}(x,y) &= \phi_a(x)\,\psi_a(y) \quad \psi_{2,1}(x,y) = \phi_b(x)\,\psi_b(y),\\ \psi_{1,2}(x,y) &= \psi_a(x)\,\phi_a(y) \quad \psi_{2,2}(x,y) = \psi_b(x)\,\phi_b(y),\\ \psi_{1,3}(x,y) &= \psi_a(x)\,\psi_a(y) \quad \psi_{2,3}(x,y) = \psi_b(x)\,\psi_b(y),\end{aligned}$$

and the imaginary parts are written similarly by:

$$\psi_k(x,y) = \psi_{3,k}(x,y) + \psi_{4,k}(x,y), \tag{14a}$$

$$\psi_{k+3}(x,y) = \psi_{3,k}(x,y) - \psi_{4,k}(x,y), \tag{14b}$$

where $\psi_{3,k}(x,y)$ and $\psi_{4,k}(x,y)$ are given by:

$$\begin{aligned}\psi_{3,1}(x,y) &= \phi_b(x)\,\psi_a(y) \quad \psi_{4,1}(x,y) = \phi_a(x)\,\psi_b(y),\\ \psi_{3,2}(x,y) &= \psi_b(x)\,\phi_a(y) \quad \psi_{4,2}(x,y) = \psi_a(x)\,\phi_b(y),\\ \psi_{3,3}(x,y) &= \psi_b(x)\,\psi_a(y) \quad \psi_{4,3}(x,y) = \psi_a(x)\,\psi_b(y).\end{aligned}$$

The real and imaginary parts of these six wavelets and their orientations with maximum sensitivity to edges are presented in Figure 16 of Selesnick et al. (2005).

This directional selectivity property provided by the 2D-DTCWT is the main ingredient for the highlight of sharp edges and distinct contours in LASCO images. Following, the methodology used to reach this objective is discussed.

IMAGE PROCESSING

The multilevel decomposition of an image by the 2D-DTCWT generates as outcomes six subimages (for each decomposition level) composed by complex wavelet coefficients representing each one of the six orientations discussed above. The analysis used here in the treatment of LASCO images is based on increasing complex wavelet coefficient magnitudes, which are within some chosen range. The wavelet coefficient magnitudes that most appear in a given subimage, or, in other words, the highest frequency wavelet coefficient magnitudes, are inside this range. Here we multiply these complex coefficients by some factor $\alpha > 0$. The coefficients outside this interval are set to zero. Thus, the contrast between edges and image background is increased.

Each subimage has its peculiarities, because each one of them captures features (edges) in specific orientations. Therefore, the distributions of wavelet coefficient magnitudes are in general different. Those distributions are obtained by means of histograms. Their x-axis are divided into half-open intervals $[2^{k-1}, 2^k)$, $k = 1, \ldots, \gamma$, where γ is the biggest integer

less than $\log_2 \|d_{\max}\|$, with $\|d_{\max}\|$ the absolute value of the largest complex wavelet coefficient of the analyzed subimage. In the y-axis are the number of times that each complex wavelet coefficient magnitude lies in the half-open interval $[2^{k-1}, 2^k)$. In the x-axis only the k values are shown. With the aid of these histograms we are able to choose the highest frequency wavelet coefficient magnitude range. For instance, consider the images shown in Figure 5 which are related to Event 1. After applying the 2D-DTCWT to the image on the left side of Figure 5, and computing the histogram of the subimage with the wavelet coefficient magnitudes oriented at –45° we obtain the histogram shown in panel (a) of Figure 6. In the case shown, the chosen range for multiplying the wavelet coefficient magnitudes by a factor α is $[2^0, 2^7)$. The other coefficients are set to zero. We do this for all subimages ($6N$ subimages, where N is the number of decomposition levels), for which we choose the proper intervals for multiplying the complex coefficients by a factor α. After these steps, the image is reconstructed by using the inverse 2D-DTCWT.

When the procedure described above is applied to LASCO images, we do not succeed a satisfactory extraction of plasma structures. The range in which the complex wavelet coefficients should be multiplied do not seem to be adequate, because we do not achieve a good contrast between the image background and the edges. Therefore, another interval has to be found. We proceed in the following way: instead of applying the 2D-DTCWT in the whole image, we choose an area containing only the plasma structure itself, i.e., the wavelet transform is performed in a zoomed in region (see Fig. 5, right panel). By doing this, we note that the histograms of the new generated subimages provide distinct intervals for the highest frequency wavelet coefficient magnitudes. As an example, panel (b) of Figure 6 shows that the interval comprising these coefficients is $[2^3, 2^7)$, which is quite different from the one chosen in panel (a) of Figure 6 ($[2^0, 2^7)$). Consequently, the reconstructed images identify in a distinctive way the coronal plasma ejections emerging from the Sun.

We can summarize the steps used for treating the images in this work as follows:

Step 1. Identify the candidate plasma structures in the image to be treated;

Step 2. Retrieve a smaller image from the original image containing this plasma structure (zoom in);

Step 3. Apply the 2D-DTCWT (for six resolution levels) in the subimage (zoomed in image);

Step 4. Identify in all the six orientations the most frequent value range of wavelet coefficient magnitudes;

Step 5. Apply the 2D-DTCWT for the entire image;

Step 6. Multiply the complex wavelet coefficients inside the intervals found in Step 4 by the factor α, and set to zero the other coefficients outside these intervals; and

Step 7. Reconstruct the image.

We chose an empirical enhancement factor $\alpha = 100$ for all images, based on a sensibility test that we performed.

RESULTS AND DISCUSSIONS

The plasma structure in Event 1 (left panel in Fig. 7) is very faint and few things can be said concerning its internal structure. However, with the implemented methodology using the range of wavelet coefficient magnitudes presented in Table 1, several internal features are much more distinguishable (right panel in Fig. 7). In this figure, the upper white arrow indicates one of these features. With the treatment, some artifacts are easily identified. For instance, white circles involving the occulter disk in LASCO-C2 images and some square-like features inside those circles. Nevertheless, the plasma structures are much better identified for a consistent characterization and further analyses. Comparing this result with the one presented in the right panel of Figure 4 of Stenborg & Cobelli (2003), one can see that the plasma structures of interest are highlighted in both cases. Due to the directional selectivity characteristic of the plasma ejection presented in this image, our result shows that the contours of the plasma structures are better identified, as indicated by both white arrows in the right panel of Figure 7.

The image shown in the left panel of Figure 8 corresponds to Event 2. On one hand, it is quite diffuse which in turn avoids an easy detection of any internal structure. On the other hand, the treated image shows this structure in much more clear details. The white arrows point to the highlighted edges. The parameters used to enhance the wavelet coefficients are presented in Table 1. The comparison between our analysis and the one made at Figure 5 of Stenborg & Cobelli (2003) should be carefully done. The images used for the wavelet processing are distinct. While we use the raw image as usual in this article, they remove the background, cosmic rays, and star fields. Furthermore, the image is rotated. In our case, we could identify the CME contours, as indicated by the white arrows, which are barely discernible in the original image. However, in Stenborg & Cobelli (2003)'s result the CME is better identified from the background.

Similarly to Event 1, the directionality of the plasma structure shown in Figure 9 is well-identified using the proposed methodology. It is noticed that all the edges become sharpened

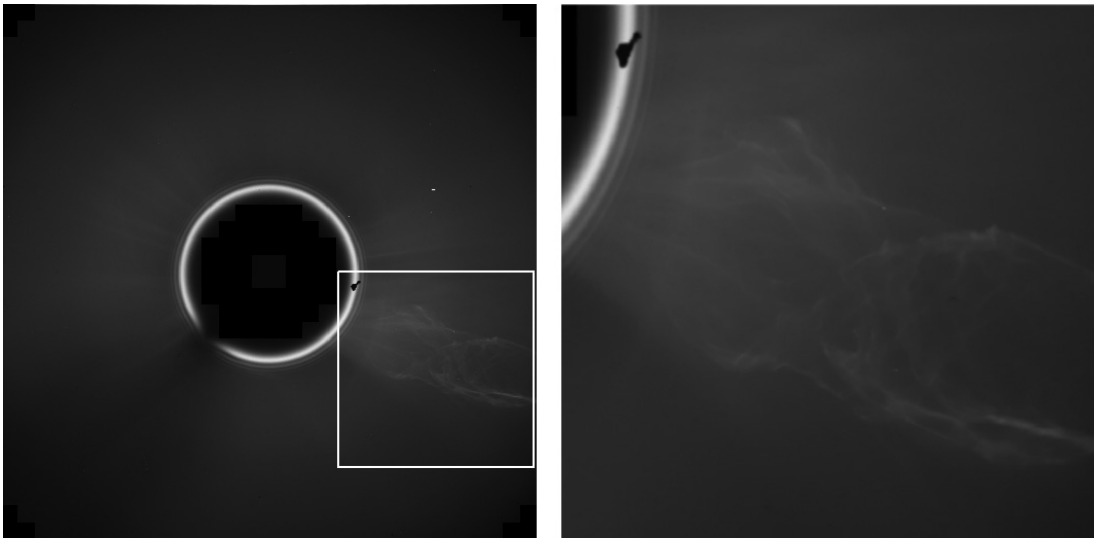

Figure 5 – Left: original image to be treated. Right: zoom in on the region containing the plasma structure (bounded by the white square). Source: SOHO archive search – http://seal.nascom.nasa.gov/cgi-bin/gui_seal.

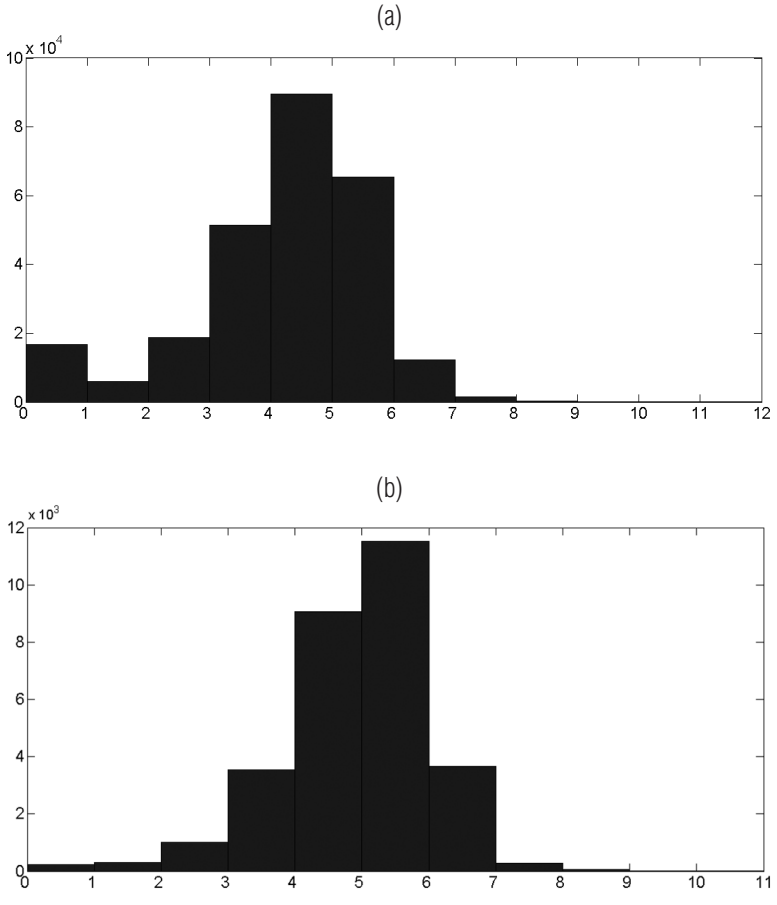

Figure 6 – Histograms of the subimages with wavelet coefficient magnitudes oriented at –45° for the first decomposition level. In (a) the subimage is obtained by performing the 2D-DTCWT in the image presented in the left panel of Figure 5, and in (b) in the image presented in the right panel of Figure 5, which corresponds to the region bounded by the white square in the left panel of Figure 5.

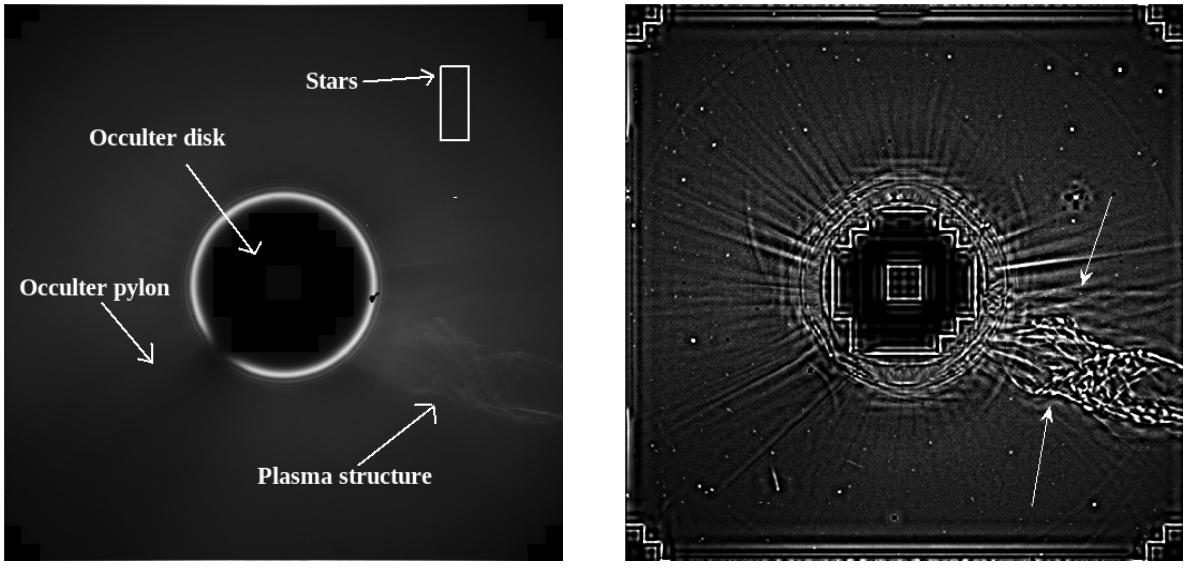

Original image Processed image

Figure 7 – Eruptive prominence obtained by LASCO-C2 on June 02, 1998 at 13:31 UT (the same in the left panel of Fig. 5).

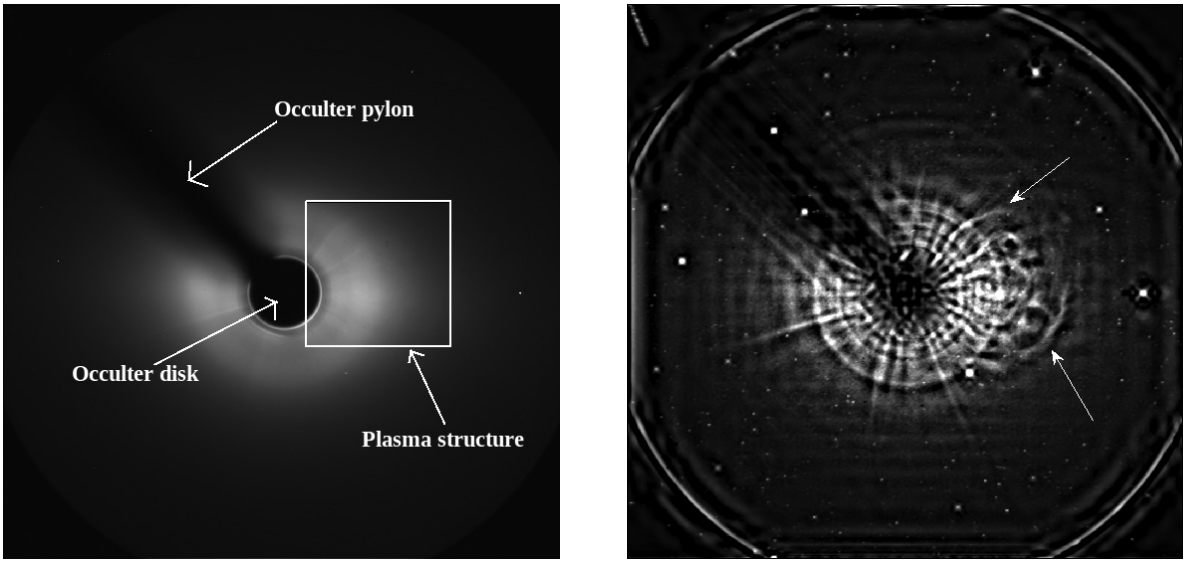

Original image Processed image

Figure 8 – CME obtained by LASCO-C3 on July 04, 2002 at 00:42 UT. The white square bounds the zoom in region.

in the treated image, which makes easier the tracking of the solar plasma. From comparison of our results with the second row of Figure 3 of Stenborg & Cobelli (2003), the same plasma structures are indeed highlighted.

SUMMARY AND CONCLUSIONS

We improved a technique using a discrete complex wavelet transform in order to unravel hidden plasma structures in originally faint and diffuse solar images.

This technique is supported on a multilevel decomposition of an image performed by a wavelet transform that uses a dual-tree of wavelet filters to compose the real and imaginary parts of complex wavelet coefficients. Then, with a particular enhancement of these coefficients, the reconstructed images have shown highlighted and sharpened edges. Highlight can make the tracking of plasma structures much easier. As a consequence, the onset times of CMEs and the associated flares from the treated images can be easily identified.

Table 1 – Range of wavelet coefficient magnitudes related to the subimages.

Event	Level(s)	Range for all orientations
1	1–2	$[2^3, 2^7)$
	3–4	$[2^4, 2^{11})$
	5	$[2^7, 2^{14})$
	6	$[2^9, 2^{16})$
2	1–3	$[2^4, 2^8)$
	4–5	$[2^5, 2^{11})$
	6	$[2^{10}, 2^{13})$
3	1–3	$[2^2, 2^7)$
	4	$[2^2, 2^{10})$
	5	$[2^{10}, 2^{13})$
	6	$[2^7, 2^{16})$

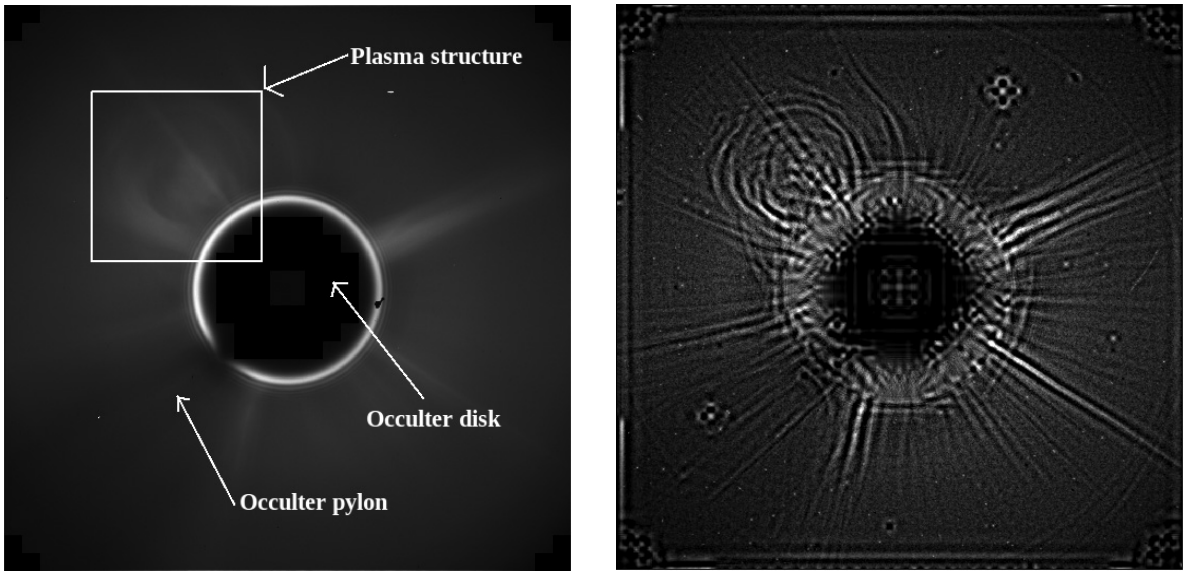

Original image Processed image

Figure 9 – CME obtained by LASCO-C2 on August 13, 2002 at 10:54 UT. The white square bounds the zoom in region.

Contributing for those kinds of techniques as used in Stenborg & Cobelli (2003), our approach is indeed useful and much simpler as compared to them. Furthermore, the computational cost of the 2D-DTCWT is much less. Success has been reached for improving the visualizations by means of well enhanced plasma structures in all treated images in this work. Moreover, other advantage is that we use raw images for the processing, with similar results for visualization as compared to more elaborated methodologies. Thus, this technique can be used as a complementary tool aiding solar physicists in a better characterization of the magnetized plasma phenomena taking place in the solar corona.

The present results encourage further work on: a) the relation between multilevel wavelet coefficients and plasma structures presented in those kind of images, b) taking advantage of the multiscale representation of the wavelet transform to use the whole image and improving the possibility of an automatic application of this technique, and c) combination of pre-processing

techniques with the proposed methodology in order to achieve even better results.

ACKNOWLEDGEMENTS

The authors thank the grants provided by FAPESP 2014/21229-9; CAPES 86/2010-29; CNPq 307511/2010-3, 486165/2006-0, 306828/2010-3, 312246/2013-7 and FAPESP 2007/07723-7; Eng. Varlei Menconi by the computational assistance (FAPESP 2008/09736-1, CNPq 302451/2013-7), Prof. Dr. Nick Kingsbury for the scientific discussions; and European Space Agency (ESA) and National Aeronautics and Space Administration (NASA) for providing the SOHO/LASCO images used in this work. SOHO is a project of international collaboration between ESA and NASA.

REFERENCES

DAUBECHIES I. 1992. Ten Lectures on Wavelets. Vol. 61 of CBMS-NSF Regional Conference Series in Applied Mathematics. SIAM, Philadelphia, PA, 357 pp.

DE RIVAZ P & KINGSBURY N. 1999. Complex wavelet features for fast texture image retrieval. In: International Conference on Image Processing. Vol. 1. pp. 109–113.

DOMINGUES MO, MENDES O & MENDES DA COSTA A. 2005. On wavelet techniques in atmospheric sciences. Adv. Space Res., 35: 831–842.

HARRISON RA. 1995. The nature of solar flares associated with coronal mass ejection. A&A, 304: 585.

KINGSBURY N. 1998. The dual-tree complex wavelet transform: A new technique for shift invariance and directional filters. In: IEEE Digital Signal Processing Workshop DSP. Bryce Canyon, USA., pp. 319–322.

KINGSBURY N. 2001. Complex wavelets for shift invariant analysis and filtering of signals. Appl. Comput. Harmon. A., 10(3): 234–253.

Recebido em 11 novembro, 2011 / Aceito em 22 maio, 2015
Received on November 11, 2011 / Accepted on May 22, 2015

MALLAT S. 1989. A theory for multiresolution signal decomposition: The wavelet representation. IEEE Transactions on Pattern Analysis and Machine Intelligence, 11: 674–693.

MALLAT S. 1991. Multiresolution approximations and wavelet orthonormal bases. Transactions of the American Mathematical Society, 315(1): 69–87.

MOURA V, DOMINGUES MO, MENDES O & PAGAMISSE A. 2011. Estudo exploratório da aplicação da transformada wavelet complexa *dual-tree* às imagens do SOHO. In: Conferência Brasileira de Dinâmica, Controle e Aplicações. Vol. 1. SBMAC, São Carlos, pp. 813–816.

SELESNICK IW, BARANIUK RG & KINGSBURY N. 2005. The dual-tree complex wavelet transform. Signal Processing Magazine, IEEE, 22(6): 123–151.

ST. CYR OC, HOWARD RA, SHEELEY JR NR, PLUNKETT SP, MICHELS DJ, PASWATERS SE, KOOMEN MJ, SIMNETT GM, THOMPSON BJ, GURMAN JB, SCHWENN R, WEBB DF, HILDNER E & LAMY PL. 2000. Properties of coronal mass ejections: SOHO LASCO observations from January 1996 to June 1998. Journal of Geophysical Research: Space Physics, 105(A8): 18169–18185.

STENBORG G & COBELLI PJ. 2003. A wavelet packets equalization technique to reveal the multiple spatial-scale nature of coronal structures. A&A, 398(3): 1185–1193.

STENBORG G, VOURLIDAS A & HOWARD RA. 2008. A Fresh View of the Extreme-Ultraviolet Corona from the Application of a New Image-Processing Technique. ApJ, 674: 1201–1206.

ZHANG J, DERE KP, HOWARD RA, KUNDU MR & WHITE SM. 2001. On the Temporal Relationship between Coronal Mass Ejections and Flares. ApJ, 559: 452–462.

ZHANG J, DERE KP, HOWARD RA & VOURLIDAS A. 2004. A Study of the Kinematic Evolution of Coronal Mass Ejections. ApJ, 604: 420–432.

APPENDIX: DTCWT FILTERS

The filters used in this work to compute the DTCWT are presented in Tables 2 and 3.

Table 2 – DTCWT odd-length filters for the first decomposition level.

n	Tree a		Tree b	
	$10^{-3}\ h_a$	$10^{-3}\ g_a$	$10^{-3}\ h_b$	$10^{-3}\ g_b$
1	–1.7578125	–0.070626395	0.070626395	–1.7578125
2	0.0000000	0.000000000	0.000000000	0.0000000
3	22.2656250	1.341901507	–1.341901507	22.2656250
4	–46.8750000	–1.883370536	–1.883370536	46.8750000
5	–48.2421875	–7.156808036	7.156808036	–48.2421875
6	296.8750000	23.856026786	23.856026786	–296.8750000
7	555.4687500	55.643136161	–55.643136161	555.4687500
8	296.8750000	–51.688058036	–51.688058036	–296.8750000
9	–48.2421875	–299.757603237	299.757603237	–48.2421875
10	–46.8750000	559.430803571	559.430803571	46.8750000
11	22.2656250	–299.757603237	299.757603237	22.2656250
12	0.0000000	–51.688058036	–51.688058036	0.0000000
13	–1.7578125	55.643136161	–55.643136161	–1.7578125
14		23.856026786	23.856026786	
15		–7.156808036	7.156808036	
16		–1.883370536	–1.883370536	
17		1.341901507	–1.341901507	
18		0.000000000	0.000000000	
19		–0.070626395	0.070626395	

Table 3 – DTCWT even-length filters for decomposition levels higher than or equal to two.

n	Tree a		Tree b	
	$10^{-3}\ h_a$	$10^{-3}\ g_a$	$10^{-3}\ h_b$	$10^{-3}\ g_b$
1	–2.2841274	2.411869457	2.411869457	2.2841274
2	1.2098942	–1.277558654	1.277558654	0.0012099
3	–11.8347945	–2.576174307	–2.576174307	11.8347945
4	1.2834570	6.628794612	–6.628794612	1.2834570
5	44.3652216	31.526377122	31.526377122	–44.3652216
6	–53.2761088	–18.156493946	18.156493946	–53.2761088
7	–113.3058864	–120.188544711	–120.188544711	113.3058864
8	280.9028632	–24.550152434	24.550152434	280.9028632
9	752.8160381	565.808067396	565.80806739	–752.8160381
10	565.8080674	–752.816038088	752.816038088	565.8080674
11	24.5501524	280.902863222	280.902863222	–24.5501524
12	–120.1885447	113.305886362	–113.305886362	–120.1885447
13	18.1564939	–53.276108803	–53.276108803	–18.1564939
14	31.5263771	–44.365221607	44.365221607	31.5263771
15	–6.6287946	1.283456999	1.283456999	6.6287946
16	–2.5761743	11.834794515	–11.834794515	–2.5761743
17	1.2775587	1.209894163	1.209894163	–1.2775587
18	2.4118695	2.284127440	–2.284127440	2.4118695

NOTES ABOUT THE AUTHORS

Vitor Moura Cardoso e Silva Souza has a BS in Physics from Universidade Federal da Bahia (UFBA, 2006), and a Ph.D. in Space Geophysics from the Instituto Nacional de Pesquisas Espaciais (INPE, 2015). Currently, is a FAPESP's post-doctoral fellow at INPE, and works with magnetospheric physics with emphasis on the magnetic reconnection phenomenon. The main research topics are: space electrodynamics, plasma physics applied to space sciences, and magnetic reconnection at Earth's and other planetary magnetospheres.

Margarete Oliveira Domingues is senior researcher at Brazilian Instituto Nacional de Pesquisas Espaciais (INPE), in the Computing and Applied Mathematics Associate Laboratory (LAC/CTE). The main interests are multiscale and wavelet analysis applied to adaptive numerical simulations and signal analysis of space physics phenomena. Had post-doctoral and visiting research positions in Europe, the United States and Japan, Ph.D. on Applied Mathematics at Universidade Estadual de Campinas (Unicamp, 2001), M.Sc. on Meteorology at INPE (1993), and a Bachelor degree in Meteorology at the Universidade Federal do Rio de Janeiro (UFRJ, 1988).

Odim Mendes is senior researcher at Instituto Nacional de Pesquisas Espaciais (INPE), in the Space Geophysics Division (DGE), in Space Science and Atmosphere Coordination (CEA). The main interests are on Space Electrodynamics, Space Plasma Processes, and Space Weather. Ph.D. (1992) and M.Sc. (1985) on Space Sciences at INPE. Bachelor's degree on Physics and teaching degree on Physics at the Universidade Federal de Goiás, Brazil (UFG, 1982). Other current activities: advisor member of Brazilian Space Weather Program (EMBRACE), deputy head of CEA Coordination, and advisor and professor for the Space Geophysics Graduation Program at INPE.

Aylton Pagamisse graduated in Mathematics from Universidade São Francisco de Assis (1983), M.Sc. degree in Mathematics from Universidade de São Paulo (1987) and Ph.D. in Applied Mathematics from Universidade Estadual de Campinas (UNICAMP) (2003). Currently, is an assistant professor at FCT-UNESP since 1987. Research interest are applications of Wavelet Transform in Digital Image Processing.